Fabrication of Nanoparticulate Inks for Applications in Printable Electronics

A. Reindl[*], S. Aldabergenova[**], E. Altin[*], G. Frank[**] and W. Peukert[*]

[*]Department of Particle Technology, Friedrich-Alexander University,
91058 Erlangen, Germany, w.peukert@lfg.uni-erlangen.de
[**] Department of Microcharacterisation, Friedrich-Alexander University,
91058 Erlangen, Germany, gerhard.frank@ww.uni-erlangen.de

ABSTRACT

Semiconducting nanoparticles were dispersed systematically in organic solvents using a variety of methods. In the case of silicon particles prepared by gas phase synthesis a high specific energy input is necessary to obtain intrinsically stable suspensions. Therefore Si nanoparticles were dispersed for 24 hours in 1-butanol using a stirred media mill. Via this process intrinsically stable suspensions of Si nanoparticles were produced. The evolution of morphology, particle size and structure was investigated by dynamic light scattering, X-ray diffraction, Raman spectroscopy, and high resolution transmission electron microscopy as a function of dispersing time. The microstructural development with varying crystallite size and crystalline volume fraction was analyzed by Raman spectroscopy and directly confirmed by transmission electron microscopy measurements. The surface chemistry of the Si nanoparticles was analyzed by diffuse reflectance infrared Fourier transform spectroscopy.

Keywords: silicon nanoparticles, stirred media mill, Raman spectroscopy, XRD, HRTEM

1 INTRODUCTION

Future progress in electronics requires the development of more powerful and compact integrated circuits and nanometer-sized devices. Since nowadays most electronic components are still built on crystalline silicon wafers, the development of printing techniques using semi-conducting nanoparticles promises inexpensive manufacture of electronic devices on flexible substrates. Additionally this approach opens new applications in the field of flexible electronics, e.g. integrated circuits for consumer products, radio frequency tags or flexible solar cells, because the advantages of flexible production of polymers are combined with the advantages of particle technology. The main impetus of this work is the fabrication of stable suspensions (with regard to aggregation) suitable for a printing process. Therefore semiconducting nanoparticles were dispersed systematically in organic solvents using a variety of methods (e.g. ultrasound, ultraturrax, and stirred media mill). In the case of silicon particles prepared by gas phase synthesis a high specific energy input is necessary to obtain intrinsically stable suspensions. Only by using a stirred media mill stable suspensions were received. The evolution of morphology, particle size and structure was investigated by dynamic light scattering (DLS), X-ray diffraction (XRD), Raman spectroscopy, and high resolution transmission electron microscopy (HRTEM) as a function of dispersing time. The microstructural development with varying crystallite size and crystalline volume fraction was analyzed by Raman spectroscopy and directly confirmed by transmission electron microscopy measurements. A specific challenge in case of Si is an increase of the oxygen content which limits the conductivity of the paste and needs to be minimized during the dispersing process. The surface chemistry of the Si nanoparticles was analyzed by diffuse reflectance infrared Fourier transform spectroscopy (DRIFTS).

2 EXPERIMENTAL

Dispersing of the silicon particles. A suspension of 20 wt.% silicon particles in 1-butanol was dispersed for 24 h using a stirred media mill (Netzsch PE 075). The temperature of the milling chamber was kept constant at 15°C, and the revolution velocity of the SiC stirrer was set to 1000 min^{-1}. Beads of yttrium stabilized ZrO_2 with a diameter of 0.3 mm were used for dispersing. For the sake of safety the oxygen concentration was kept below 7% during the milling process by using a glove-box flooded with nitrogen. After 24 h of grinding the milling beads were separated from the SiNP by sieving and a stable suspension of SiNP in 1-butanol was received. During the milling process samples of four drops of suspension were taken out of the milling chamber at defined intervals and diluted with 5 ml of 1-butanol for measuring the evolution of the particle size distribution with DLS. Additionally 5 ml of suspension were taken out of the milling chamber after 2, 4, 6, 10 and 24 hours in order to prepare samples for XRD, TEM, Raman spectroscopy, elemental analysis and BET measurements. 1-Butanol was evaporated and the samples were dried in vacuum for 24 h at 100°C.

Dynamic Light Scattering (DLS). The particle size distributions of the samples collected during the milling process were obtained by measuring the intensity fluctuation of the scattered light of a 3 mW-semiconductor laser (λ = 780 nm) using a Honeywell Microtrac Ultrafine Particle Analyzer (UPA 150).

X-Ray Diffraction. XRD data was collected using a Siemens D500 powder diffractometer equipped with a

curved graphite secondary monochromator (0.05° slit width) in the diffracted beam arm and using Cu K_α radiation (λ = 0.15406 nm).

Raman spectroscopy. Unpolarized Raman scattering was measured in back scattering configuration at room temperature in a HR800 integrated Raman system using the 415.5 nm line from an Ar^+ laser. One drop of the SiNP dispersion was placed on an Al sample holder and the solvent was evaporated. The Laser power on the samples was reduced to a minimum, < 10 mW, in order to avoid artifacts due to sample heating.

Transmission Electron Microscopy (TEM). The TEM and HRTEM images were obtained using a Philips CM 30 T/STEM microscope and a Philips CM 300 UltraTwin microscope, respectively. The measurements were carried out at an acceleration voltage of 300 kV in bright-field mode.

Diffuse Reflectance Infrared Fourier Transformation Spectroscopy (DRIFTS). The DRIFT spectra of the SiNP were recorded on a Varian FTS 3100 FTIR spectrometer equipped with a Pike Technologies EasiDiff accessory.

3 RESULTS AND DISCUSSION

The untreated SiNP obtained from Degussa Creavis consist of primary particles of nearly spherical shape with a diameter of approximately 100 nm (see Fig. 1). The TEM image in Fig. 1 reveals that the primary particles are interconnected via sinter bridges forming µm-sized agglomerates. Since the SiNP were fabricated by gas phase synthesis in a hot-wall reactor [1] the solid bridges either developed by sintering or surface growth. Due to the formation of the large agglomerates the SiNP do not generate stable suspensions while dispersing with ultrasound or ultraturrax.

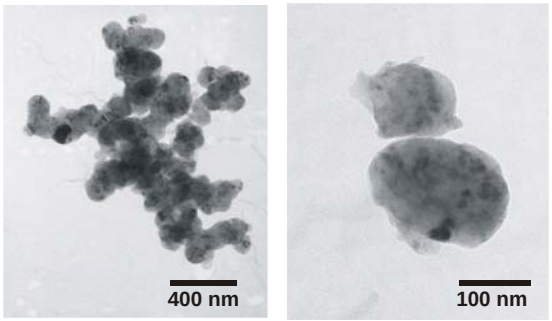

Figure 1: Untreated SiNP (left) and dispersed SiNP (right).

Hence, successful processing of the SiNP requires methods with a high specific energy input e.g. a stirred media mill. Therefore the SiNP were wet-ground in 1-butanol as described before. Stable suspensions of SiNP were received after 6 h of dispersing. Obviously the solid sinter bridges were destroyed during the dispersing process leaving behind smaller, individual particles as exemplarily shown by the TEM micrograph in Fig. 1b. DLS measurements revealed that the stable suspensions consist of individual particles or small aggregates with a balanced mean diameter of the volumetric density distribution $x_{1,3}$ of approximately 160 nm. The evolution of $x_{1,3}$ during the dispersing process monitored by DLS is exhibited by Fig. 2. Within the first hour of dispersing $x_{1,3}$ rapidly decreases from 1690 nm to 450 nm which indicates that most sinter bridges break during that time period. Between 1 and 6 h of grinding the aggregate size decreases exponentially to 170 nm and stays nearly constant within the remaining milling process due to the equilibrium of breakage, agglomeration, and desagglomeration [2, 3].

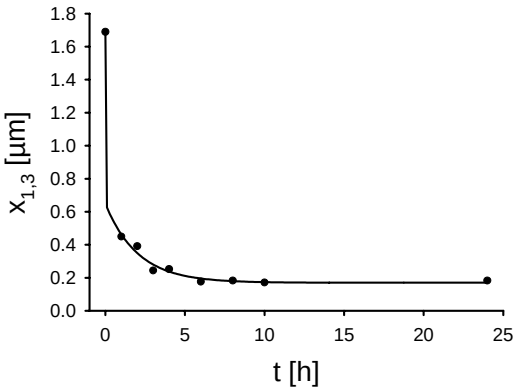

Figure 2: Evolution of $x_{1,3}$ with dispersing time.

After investigating the development of the particle size and morphology, XRD measurements were conducted in order to examine the evolution of the SiNP structure. In Fig. 3 the evolution of the XRD-patterns of the SiNP successively collected during the milling process is depicted. With increasing dispersing time the diffraction peaks exhibit line broadening and therefore an increase of the full with at half maximum (FWHM). Additionally an increase of the amorphous background and a significant decrease in intensity of the diffraction peaks is observed with proceeding dispersing time (see inset Fig. 3). The line broadening is due to a decreasing crystallite size and strain caused by internal stress. However, in the lower nanometer range the main contribution of the line broadening is determined by the decrease in crystallite size and therefore the effect of strain caused by stress is excluded in the following. According to the Scherrer equation, the width of the XRD lines is inversely proportional to the size *d* of the crystallites. One can infer the size of the Si nanocrystallites using the formula.

$$d = \frac{0.9\lambda}{B\cos\theta} \qquad (1)$$

where *B* is the full width at the half maximum of the XRD peak and λ is the wavelength in nanometer. The crystallite size estimated after the width of the Si (111)

peak decreased from 18 nm to 10 nm during the dispersing process.

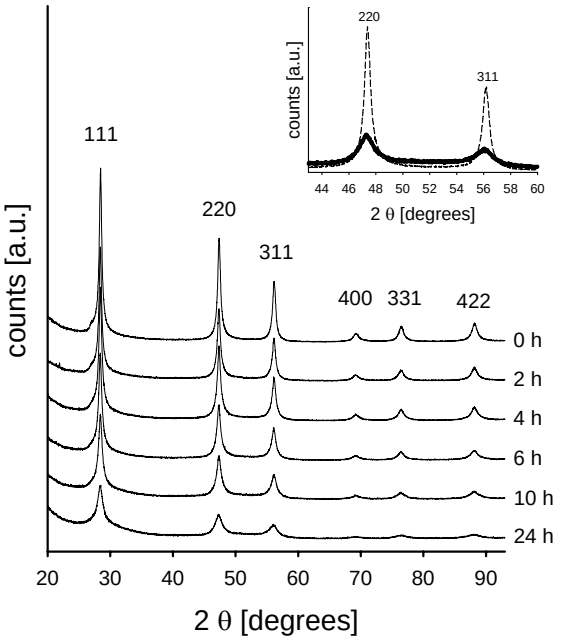

Figure 3: Evolution of the XRD patterns with disp. time.

An alternative technique presently used to determine the size and concentration of nanocrystallites in silicon, besides XRD and HRTEM, is Raman spectroscopy. Fig. 4 shows the evolution of the Raman spectra of the Si nanoparticles with dispersing time. All spectra were recorded at the same instrumental conditions, i.e. laser power, laser wavelength, and spectrometer settings. The vertical line in Fig. 4 marks the peak position of the c-Si TO phonon mode of a polycrystalline Si wafer measured under the same experimental conditions for reference. The peak of the c-Si TO phonon mode located at around 520 cm^{-1} dominates all spectra. The peak position shifts slightly towards smaller frequencies with an increasing time of dispersing. Because of the fact that this shift is systematic, one can expect that the red shift of the position of the c-Si TO phonon occurs due to a constant decrease of the crystallite size according to quantum confinement. The peak shift ($\Delta\omega$) of the c-Si TO phonon mode of the SiNP compared to c-Si TO phonon mode of the reference was 1.4 cm^{-1} after 2 h of dispersing and increased to 2.8 cm^{-1} after 24 h of dispersing. The mean crystallite size d of the SiNP was calculated using the formula [4]

$$d = 2\pi(B/\Delta\omega)^{1/2} \qquad (2)$$

where B is the FWHM of the c-Si TO mode estimated by a fitting procedure. The mean crystallite sizes determined by the Raman data were compared to the ones determined by the XRD data (see Fig. 6) and the results agreed to a reasonable extent. Both methods indicated a constant decrease of the crystallite size with an increasing dispersing time.

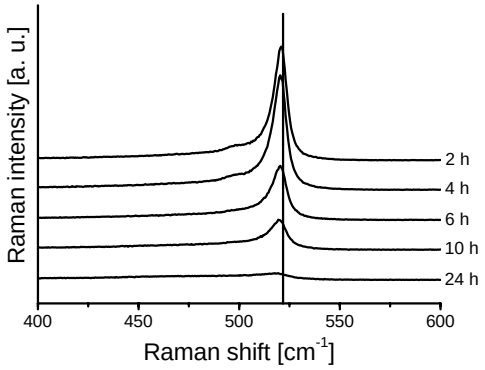

Figure 4: Evolution of the Raman spectra with disp. time.

In addition to the estimation of the crystallite size Raman spectroscopy allows the quantification of the crystalline volume fraction of mixed phase Si. However, a careful analysis of the spectral details was necessary for this task. All spectra depicted in Fig. 4 show that the systematic red shift of the c-Si TO peak is accompanied by the broadening of the peak and loss of intensity. The c-Si TO peak is asymmetric and shows a "shoulder" towards the low frequency region. With proceeding time of dispersing the intensity of the broad features in the low frequency region increases as the intensity of the sharp crystalline peak significantly decreases, which indicates that the increase of amorphous Si fraction occurs at the expense of the Si crystallites.

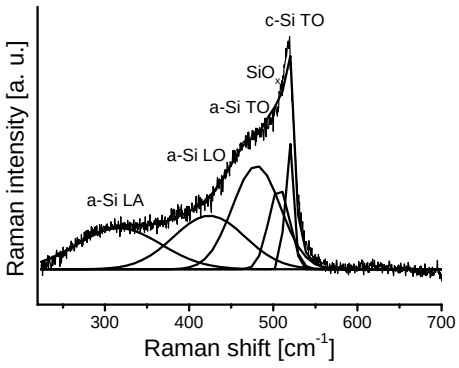

Figure 5: Raman spectrum of SiNP disp. for 24 h.

For accurate analysis of the spectral details the spectra were fitted with 5 Gaussian peaks. The fitting result for one spectrum, in this case the one of the SiNP dispersed for 24 h, is depicted exemplarily in Fig. 5. The FWHM and the

positions of the peak at 505 cm^{-1}, as well as of the three peaks attributed to the modes of a-Si, were kept constant throughout the fitting procedures of all Raman spectra. Using the fitting results one can establish the relation between the integrated Raman intensity and the volume fraction of the nanocrystalline phase x_c. This relation is usually written in the form [5, 6]

$$x_c = \frac{I_c / I_a}{\gamma + I_c / I_a} \tag{3}$$

where I_c and I_a are the integrated Raman intensities of the crystalline and amorphous phase respectively. The scattering factor γ may vary from 0.1 to 1 and was calculated using the formula [7]

$$\gamma = 0.1 + e^{-(L/25nm)} \tag{4}$$

where L is the crystallite diameter. For I_c and I_a the integrated intensities of the c-Si TO mode and the a-Si TO mode were taken into account respectively. Due to the increase of the peak shift $\Delta\omega$ of the c-Si TO mode compared to the reference a decreasing crystallite size L from 15.4 nm to 12.9 nm with proceeding dispersing time was calculated. Compared to the change in crystallite size the change in the volume fraction of the nanocrystalline phase x_c from 75 % to 24 % was drastic. HRTEM measurements complemented the results obtained by XRD and Raman spectroscopy.

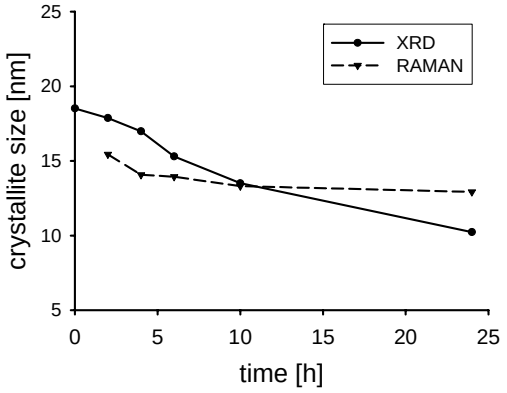

Figure 6: Crystallite size determined by XRD/Raman

Besides investigating the development of particle size, morphology and structure the development of oxide formation during the dispersing process is of fundamental interest. Therefore the SiNP were examined using diffuse reflectance infrared Fourier transform spectroscopy (DRIFTS). The DRIFTS show characteristic vibrational modes that indicate the presence of an oxide with a complex stoichiometry: several Si-H streching and bending modes with a varying number of O neighbor atoms [8] from 2000 - 2200 cm^{-1} and a broad band in the region from 1000 – 1100 cm^{-1} accounting for Si-O streching modes of $Si\text{-}O_y\text{-}Si_{4-y}$ complexes [9]. A band around 500 cm^{-1} can be assigned to the Si-O-Si out-of-plane bond-rocking motion [10]. Additionally the spectra contained strong and characteristic bands that are associated with residual 1-butanol: C-H streching, C-H bending and O-H stretching. Presumably 1-butanol is strongly bound to the SiNP surface during the dispersing process.

4 CONCLUSIONS

SiNP were successfully dispersed in 1-butanol with a stirred media mill. Intrinsically stable suspensions were received after 6 h of dispersing. Details of the microstructural development were revealed by XRD, Raman spectroscopy, and HRTEM measurements. A constant decrease of crystallite size from about 18 nm to 10 nm, together with a constant increase of amorphization from 25 % to 76 % was observed. DRIFTS measurements indicated the formation of an oxide with a complex stoichiometry in all samples examined. Careful analysis of the development of particle structure and oxide formation as a function of dispersing time enables the optimization of the fabrication of conductive nanoparticulate inks in regard to the desired properties in printable electronics.

REFERENCES

[1] H. Wiggers, R. Starke, P. Roth, Chem. Eng. Technol. 24, 261 (2001).

[2] M. Sommer, F. Stenger, W. Peukert, N. J. Wagner, Chem. Eng. Sci. 61, 135 (2006).

[3] F. Stenger, S. Mende, J. Schwedes, W. Peukert, Pow. Tech. 156, 103 (2005).

[4] Y. He, C. Yin, G. Cheng, L. Wang, X. Liu, G. Y. Hu, J. Appl. Phys. 75, 797 (1994).

[5] V. G. Golubev, V. Y. Davydov, A. V. Medvedev, A. B. Pevtsov, N. A. Feoktistov, Phys. Solid State 39, 1197 (1997).

[6] A. T. Voutsas, M. K. Hatalis, J. Boyce, A. Chiang, J. Appl. Phys. 78, 6999 (1995).

[7] E. Bustarret, M. A. Hachicha, M. Brunel, Appl. Phys. Lett. 52, 1675 (1988).

[8] D. V. Tsu, G. Lucovsky, B. N. Davidson, Phys. Rev. B 40, 1795 (1989).

[9] I. P. Lisovskii, V. G. Litovchenko, V. B. Lozinskii, S. I. Frolov, H. Flietner, W. Fussel, E. G. Schmidt, J. Non-Cryst. Solids 187, 91 (1995).

[10] G. Lucovsky, J. Yang, S. S. Chao, J. E. Tyler, W. Czubatyj, Phys. Rev. B 28, 3225 (1983).